HHS Public Access

Author manuscript

Nat Cell Biol. Author manuscript; available in PMC 2009 June 01.

Published in final edited form as:

Nat Cell Biol. 2008 December ; 10(12): 1393–1400. doi:10.1038/ncb1797.

Fluctuations of intracellular forces during cell protrusion

Lin Ji, **James Lim**, and **Gaudenz Danuser**

Department of Cell Biology, The Scripps Research Institute, 10550 North Torrey Pines Road, La Jolla, CA 92037

Abstract

We propose a model to infer from live cell images of actin filament (F-actin) flow intracellular force variations during protrusion-retraction cycles of epithelial cells in a wound healing response. To establish mechanistic relations between force development and cytoskeleton dynamics, force fluctuations were correlated with fluctuations in F-actin turnover, flow, and F-actin-vinculin coupling. Our analyses suggest that force transmission at focal adhesions (FA) requires binding of vinculin to F-actin and integrin (indirectly), which is modulated at the vinculin-integrin but not the vinculin-F-actin interface. Force transmission at FAs is co-localized in space and synchronized in time with transient increases of the boundary force at the cell edge. Surprisingly, the maxima in adhesion and boundary forces lag maximal edge advancement by ∼40 s. Maximal F-actin assembly is observed ∼20 s after maximal edge advancement. Based on these findings, we propose that protrusion events are limited by membrane tension and that the characteristic duration of a protrusion cycle is determined by the efficiency in reinforcing F-actin assembly and adhesion formation as tension increases.

Introduction

Cell protrusion requires the precise integration of polymerization of actin filaments (F-actin) at the leading edge1-3, coupling of F-actin to the extracellular matrix (ECM)4-6, and contraction7, 8. While each of these force-generating processes has been characterized in great molecular detail, their coordination in space and time and their relationships to F-actin network dynamics are poorly understood. To study these aspects, *intracellular* forces must be mapped at the spatial and temporal scales of protrusion dynamics9.

Methods to probe forces with subcellular resolution have employed traction force microscopy (TFM)5, 10-12, optical traps13, 14, or atomic force microscopy15, 16. However, these measurements capture only the *extracellular* portion of cell-generated forces. They neither reveal the location of cell contraction nor the force balance between contraction and edge propulsion. In addition, they are mechanically invasive and offer limited insights of spatial force relationships, precluding undistorted analyses of force regulation.

Correspondence to: Gaudenz Danuser, gdanuser@scripps.edu.

Here, we propose to map with single-micron resolution force fluctuations during protrusion and retraction cycles of epithelial cells based on a mechanical model that relates variations in F-actin network flow tracked by fluorescent speckle microscopy (FSM) to variations in intracellular force levels. We found that adhesion force transients were inversely correlated with the motion coupling of F-actin and vinculin speckles4. This indicates that cell adhesion is regulated at the vinculin-integrin but not the F-actin-vinculin interface. Spatiotemporal correlation of force fluctuations with F-actin assembly, flow and cell edge movements established an inverse relationship between edge advancement and boundary force, suggesting that membrane tension limits cell protrusion in a dynamic cycle whose time scale is determined by putative feedback between tension increase and F-actin assembly.

Results

Principles of force prediction and model assumptions

Forces in lamellipodium and lamella of epithelial cells were inferred from the F-actin network flow field $\boldsymbol{u}(\boldsymbol{x}, t)$ measured by quantitative FSM17, 18 (Fig. 1a). Spatiotemporal gradients in direction and/or magnitude of the flow vectors indicate local deformations of the F-actin network (Fig. 1b) associated with intracellular forces (Supplementary Note 1). Our goal was to predict the distribution of boundary forces $\boldsymbol{F}_{\mathrm{I}}$ at the leading edge, $\partial\Omega_{\mathrm{LE}}$, and contraction and adhesion forces $\boldsymbol{F}_{\mathrm{II+III}}$ inside the cellular region, Ω, that would optimally explain the measured network deformation. The concept of force reconstruction can be understood by analogy of a Hookean spring under tension (Fig. 1c). The force F required to extend a spring is proportional to the extension u relative to the relaxation length L, i.e. the external force is *balanced* by spring-internal stresses. The ratio $\varepsilon=u/L$ is referred to as the strain. Knowing the spring constant k and the strain, the force is $F=k\cdot\varepsilon$.

While with a spring the material properties are well-defined and constant, they are difficult to calibrate for an F-actin network and they continuously change as the cell migrates. To date, no method exists to probe the material properties of F-actin in living cells at the spatial and temporal scale of FSM data. To overcome this information gap, we relied our analysis on four central assumptions: i) At the length scale of live cell light microscopy ($\sim$0.5 - 1μm) F-actin networks are locally isotropic and continuous; ii) At the time scale of FSM movies (1-10 sec/frame) the response of F-actin networks to force changes is predominantly linear elastic19 (Supplementary Note 2); iii) At any time point the F-actin network is in a resting quasi-steady state; and iv) The mechanical coupling of the lamellipodium and lamella actin networks20, 21 is sufficiently rigid to approximate the actin cytoskeleton at the leading edge as a single material entity (Supplementary Note 3).

There are two main sources of material anisotropy in F-actin networks: filament branching and filament bundling. Branching occurs an order of magnitude below the length scales observed by light microscopy. As indicated by our results below, filament bundles are often large enough to be resolved explicitly as force-bearing and/or force generating structures between isotropic regions. Thus, the simplification of an isotropic network mostly neglects small alignments of actin filaments which do not affect force predictions on a length scale of $\sim$1μm.

In view of the mainly elastic behavior of F-actin over δt = 1 - 10 s, we describe the flow changes between consecutive frames of FSM movies as the *transiently elastic* response of the network to force application. Over $\Delta T \sim 100$ s, the network exhibits a plastic response as filaments disassemble and reassemble22, 23. Stresses produced by shorter-term force transient are continually relaxed. The characteristics of such a material model are illustrated in Figure 1d. Thus, force fluctuations can be predicted by analysis of the spatial and temporal variation of F-actin flow assuming quasi-steady state material properties.

Inference of force transients

F-actin flow fields were recorded with multi-fluorophore speckles, allowing the measurement of F-actin flow gradients over sub-micron distances17. Using the continuum mechanical model and numerical force inference discussed in Supplementary Notes 4 and 5 we predicted maps of intracellular force transients (Fig. 2a). These maps indicate on a relative scale force variations between different cellular locations and between time-points. Inference of absolute force levels would require measurements of the elastic properties of lamellipodial and lamellar F-actin structures. No method exists to accomplish this at the length scale of flow gradients. Nevertheless, relative force levels were sufficient to examine the modulation of contraction, adhesion and boundary forces during protrusion and retraction events.

Boundary forces (Fig. 2a, region I) reflect the pressure the growing F-actin network experiences at the cell edge. A region of forward directed force vectors (Fig. 2a, region II) indicates the resistance F-actin retrograde flow experiences near the cell edge. A region of opposing retrograde and anterograde force vectors localizes ~10 μm behind the cell edge (Fig. 2a, regions III and IV). Retrograde flow in region III is accompanied by forces parallel to the flow direction. Slower anterograde flow in region IV is accompanied by forces of almost similar magnitude. Conversely, fast flow speeds between regions II and III (Fig. 2b) are accompanied by low force levels. These observations illustrate ‘flow-speed’ and ‘force-strength’ are not directly related. Strong forces occur in regions with high strain, which is independent of the flow speed.

The force reconstruction algorithm distinguishes between boundary forces $\boldsymbol{F}_{\mathrm{I}}$ and domain forces $\boldsymbol{F}_{\mathrm{II+III}}$. To infer the contribution of adhesion and contraction to the domain force transients, we defined the *cone rule* (Figure 2c, d; Supplementary Note 6) assuming that in adhesion-dominated regions forces are anti-parallel to network flow while force and flow vectors are approximately parallel in contraction-dominated regions. Accordingly, in Figure 2e the lamellipodium at the cell edge is an adhesion-dominant region whereas contraction-dominant regions distribute throughout the lamella. Figure 2e-I highlights a mixed-force region where adhesion forces are gradually overcome by contraction forces as the flow field is deflected into centers of high contractile activity. Further evaluation of the proposed model and numerical approach to force reconstruction was performed on simulated force fields with simulated measurement noise (Supplementary Note 7). We also tested the colocalization of contraction forces with myosin-II motors (Supplementary Note 8, Fig. S4 and Video 1) and of adhesion forces with eGFP-vinculin (Fig 3a), following previous reports of correlations between vinculin density with traction force5, 24. Overall, these

analyses established the possibility to predict from F-actin flow adhesion, contraction, and boundary force transients that mediate morphological changes during protrusion and retraction.

Strong adhesion forces require simultaneous linking of vinculin to F-actin and integrins

Predicted high adhesion forces co-localized with high eGFP-vinculin intensity only in regions where the cell edge was in a protruding state (Fig 3a). High eGFP-vinculin signals could also be observed in the absence of adhesion forces (asterisks Fig. 3b, upper panel). Kymograph analyses showed local cell edge retraction and sliding of the FA site in these regions (Top and Bottom). In contrast, the adhesion site in the Middle region is stationary over ∼15 minutes and the cell edge advances by ∼7 μm between minute 6 and 9 (Video 2). Previous analyses of the relative motion between F-actin and vinculin suggested that the motion coupling of spectrally distinct actin and vinculin speckles, assessed by the Direction Coupling Score (DCS) and the Velocity Magnitude Coupling Score (VMCS)4, increased concurrently with the sliding of the FA site (green and blue curves in Fig. 3b, lower-right panel, T and B). In contrast, DCS and VMCS values fluctuated at a medium level when cells protruded (Fig. 3b, lower-right panel, M). Based on this data it was proposed that in protruding regions vinculin would bind transiently and directly or indirectly to both F-actin and integrins, while in retracting regions the link to the integrins would be selectively released. Thus, vinculin would be a key component of a regulatable slippage clutch that transmits forces from the F-actin network to the ECM.

To test this hypothesis, further mechanical evidence was needed to show that changes in the motion coupling between vinculin and F-actin would alter force transmission. By combining intracellular force reconstruction and multispectral speckle analysis we found that the predicted adhesion force increased when the motion of vinculin speckles was partially coupled to the F-actin flow, and vanished when the motion of vinculin and F-actin speckles was fully coupled (compare time courses of VMCS/DCS with time courses of adhesion force in Fig. 3b-lower right panel and Fig. 3c). Importantly, the only information used to predict these adhesion force changes was the temporal variation of F-actin flow gradients. Thus, force predictions and motion coupling of F-actin and vinculin speckles are truly independent variables reporting the dynamic state of adhesions.

Coupling of predicted adhesion and boundary forces

Efficient cell protrusion requires a balance of propulsive forces at the leading edge and adhesion forces behind the protruding sector. To investigate the coordination of propulsive and adhesive forces, we performed a spatiotemporal correlation analysis of boundary and adhesion force transients along the leading edge. Predicted force magnitudes were averaged in probing windows that moved with the cell edge (Fig. 4a; Video 3) and were copied column-by-column into a color-coded matrix (blue - weak forces; red - strong forces) referred to as *activity maps* (Fig. 4b). Activity maps of adhesion and boundary forces show similar spatiotemporal organizations. Both forces drop in bottom and top sectors at 4 min and 10 min, respectively (arrows). These events coincide with the onset of FA sliding (arrows in Fig. 3b).

To quantify the coupling of predicted boundary and adhesion force transients, we computed their cross-correlation both as a function of temporal and spatial shifts. The resulting cross-correlation score map indicates whether and by how much the two forces are co-modulated (Fig. 4c). The position of the maximal correlation score determines the time lag between adhesion and boundary force transients (horizontal displacement of the peak from 0) and the spatial shifts between force transients along the cell leading edge (vertical displacement of the peak from 0). A sharp peak at zero shifts was obtained: when the boundary force is high, the adhesion force is high, and vice versa. This finding suggests that adhesions adjacent to the leading edge balance propulsive forces while network contraction contributes much less to the adhesion forces in this region.

Timing of force modulation relative to morphological and cytoskeletal dynamic events

Next, we applied spatiotemporal cross-correlation analysis to identify the timing between predicted boundary/adhesion forces, velocities of cell edge movement9; and rates of F-actin assembly/disassembly23. For each of these parameters an activity map was constructed, in this example using 24 probing windows (Fig. 5a). The cell exhibits a burst of forward motion in a ∼5 μm-wide sector of the leading edge, while remaining stationary or undergoing slow retraction in other sectors (Video 4). The analyses confirmed that boundary and adhesion forces are co-localized and synchronized (Fig. 5a-left, b-III/IV and c-i). Visual inspection of time-lapse sequences of adhesion/boundary force maps and maps of F-actin assembly/disassembly suggested that the forward movement of the cell edge was accompanied by transient increases in force and F-actin assembly (Fig. 5a-right). Cross-correlation analysis revealed that the increase in boundary/adhesion force lags the increase in F-actin assembly by ∼20 sec (Fig. 5a-right, b-III/IV/V and c-ii, Video 4). Variations in assembly/disassembly rates lag behind the corresponding variations in protrusion/retraction velocities also by 20 sec (Fig. 5b-I/V and c-iii). Thus, boundary force increases should be delayed by 40 sec relative to the corresponding protrusion event, as confirmed by cross-correlation (Fig. 5b-I/IV and c-iv).

Together, these analyses established the following sequence of events during cell protrusion (Fig. 5d). Upon initial activation of F-actin assembly, the leading edge advances rapidly against low plasma-membrane tension (low boundary force). Hence, work produced by F-actin polymerization is mostly converted cell edge advancement and the protrusion velocity is significantly higher than retrograde flow (Fig. 5b-I/II). 20 sec after maximal protrusion F-actin assembly reaches the maximum rate. During this period boundary and adhesion forces begin to rise indicating a tension increase in the expanding plasma-membrane. Boundary and adhesion force maxima are reached 20 sec later. At this time-point edge advancement is largely stalled and substantial work by F-actin polymerization is converted into retrograde flow. Hence, fastest retrograde flow rates were reached concurrently with the peak in boundary force (Fig. 5c-v). The internal consistency among these events provides additional validation of the force predictions that corroborate with independent measurements of cell edge movement and F-actin turnover.

Discussion

Morphogenic cell functions require precise spatiotemporal coordination of intracellular forces, often in concert with local cytoskeleton reorganization. We implemented a method to infer intracellular force fields from the *transiently elastic* response of the F-actin network observed by actin speckle flows. Inference of absolute force distributions would require knowledge of network elasticity and prestress. Several approaches have been proposed to probe these parameters in living cells25-28; however, none of them match the resolution of FSM or capture the properties of thin protruding lamella and lamellipodia, which are of interest here.

Without a precise profile of network material properties, it is still possible to estimate force transients on a relative scale. Variations of the elastic modulus up to one order of magnitude have no qualitative effect on force predictions in lamella and lamellipodia (Supplementary Note 8). This robustness originates in the different length scales of network deformation and material property changes. Network deformations vary over less than a micron, material properties in lamellipodium and lamella vary over 5-10 microns. Thus, the flow gradients resolved by speckles (distances of ∼500 nm) are dominated by force transients. While the method is limited to the specific space- and time-scales captured by FSM its particular strength is that forces are probed passively and without mechanical influence on the cell. Hence, force fluctuations can be tracked during rapid processes such as cell edge protrusion.

We exploited these capabilities to analyze how force transmission from the cytoskeleton to the ECM relates to vinculin-F-actin interactions within focal adhesions as observed by motion coupling of vinculin and actin speckles4. Vinculin molecules may undergo transitions between four binding states (Fig. 3d, panel I): a) direct binding to F-actin only; b) indirect binding to integrin only (e.g. via talin29); c) simultaneous binding to F-actin and integrin; and d) binding to neither. State d) does not contribute to speckle images30. State c) is likely short-lived compared to states a) and b), but critical for transmitting intracellular forces to the ECM4. Partial coupling of vinculin to actin speckle motion, as observed in stationary FAs behind protruding edges, could be associated with both scenarios I (clutch engaged) and II (clutch disengaged). Similarly, full coupling, as observed in sliding FAs during edge retraction, could be associated with both scenarios III (clutch disengaged) and IV (clutch weakly engaged). Thus, the coupling of speckle motion is not representative of the state of force transmission.

By relating speckle motion coupling to force generation in individual FAs we excluded scenarios II and IV. Predicted adhesion forces were high when the motion of vinculin speckles is only partially coupled to F-actin speckle flow. Tight coupling of vinculin and actin speckle flows results in almost complete loss of force (asterisks in Fig. 3b-lower-right panel and Fig. 3c-Bottom sector), suggesting that vinculin is the core of a molecular clutch that modulates force transmission from the contractile cytoskeleton to the ECM.

We then scrutinized relationships between predicted adhesion force and boundary force during protrusion events. At the time scales of our analyses the two forces are tightly co-modulated. First, this means that contraction contributes little to the force balance at the

leading edge, confirming previous conclusions from F-actin flow data alone20. Second, this means that between cell boundary and adhesion sites forces are transmitted instantaneously. Importantly, this prediction is not by construction of the mathematical model. Adhesion and boundary force predictions are numerically independent if network deformations at FAs and at the boundary are resolved separately (see Eq. S4 - S6). Network deformations were calculated between neighboring speckles, i.e. over 0.5-1μm, significantly less than the 2-3μm between cell boundary and adhesion sites (Supplementary Note 7). The instantaneous coupling of adhesion and boundary forces confirmed that over a few seconds lamellipodium and lamella are mechanically well-integrated and predominantly elastic (Supplementary Note 3).

Adhesion and boundary forces gradually increase during a protrusion event while the rate of edge advancement decreases. Edge advancement is stalled at the time point of maximum boundary force (~40 s after fastest edge advancement; Fig. 5d). This suggests that the rate of cell protrusion is limited by increasing tension in the plasma-membrane, a result that has been difficult to obtain by direct measurements of boundary forces16. Consistent with this interpretation, maximal F-actin retrograde flow coincides with the boundary force maximum (Fig. 5c-v, Fig. 5d), suggesting that upon reaching a tension level precluding further expansion of the plasma-membrane, the work by F-actin assembly is converted into retrograde flow. The onset of a new protrusion cycle requires relaxation of tension, for instance by lipid flow within31 or vesicular transport to the plasma-membrane32, 33.

Multiplication of the sum of edge motion and F-actin flow velocities (Fig. 5b-I/II) with the predicted boundary force (Fig. 5b-IV) yields the instantaneous power output of the protrusion machinery (Fig. 5b-VI). Given the time-shifts between edge movement and boundary force, maximal power output is expected to fall between the peaks of protrusion velocity and force. Indeed, the cross-correlation score between edge velocity and power peaks at -20 s (Fig. 5c-vi; Fig. 5d). Power output is energy production per time unit. The energy required to advance the cell edge is presumably harnessed from the binding energy of monomers newly incorporated into the network34. Accordingly, the power output, but not the protrusion velocity, is expected to rise concurrently with the rate of F-actin polymerization. To test this hypothesis, we used FSM to generate activity maps of F-actin assembly and disassembly (Fig. 5b-V). Cross-correlation between these activities and edge velocity confirmed that the peak in F-actin assembly is delayed by 20 s to the peak in protrusion velocity (Fig. 5c-iii). Consistently, the correlation score between power output and F-actin assembly is maximal at 0 s (Fig. 5c-vii).

In summary, contrary to a model where protrusion rates are directly related to actin assembly rates1, relatively low assembly rates at the onset of a protrusion cycle are sufficient to rapidly push forward the plasma-membrane. The rate of polymerization increases as the plasma-membrane expands, possibly mediated by tension-feedback. 20 s after peak protrusion, tension reaches a threshold level beyond which the efficiencies of feedback and/or F-actin assembly begin to decay. 40 s after peak protrusion, the resistance of the plasma-membrane is too high to allow further advancement. The interval from feedback activation at low tension to feedback inhibition under high tension sets the time scale of a cell protrusion cycle. The molecular details of feedbacks between membrane

tension and F-actin assembly remain elusive. Possible mechanisms include curvature-dependent transport and/or scaffolding of signaling molecules within the plasma-membrane35, 36. Unraveling these connections will critically depend upon in situ measurements of the timing between forces, feedback signals, and cytoskeleton dynamics. The presented force reconstruction will provide an unprecedented source of high-resolution data to achieve this goal.

Methods

Cell culture and microinjection

Ptk1 cells were cultured in Ham's F-12 medium (GIBCO), supplemented with 10% FBS, 100 U/ml penicillin, 0.1 mg/ml streptomycin, 1 mM sodium pyruvate, and 2 mM of L-glutamine. The cells were incubated at 37°C/5% CO_2. Cells were plated on acid-washed glass coverslips for 20 - 24 hours before experiments. To reduce the effects of photobleaching, 1.0U of oxyrase (Oxyrase Inc.) were added to 1 ml of culture medium. Cells were microinjected with X-Rhodamine-conjugated actin using an Eppendorf Transjector 5246 (Eppendorf Inc.) into the cell cytoplasm at 0.5 mg/ml, as described in37. Plasmid DNA encoding eGFP-vinculin was nucleoinjected as described in4. Full length myosin regulatory light chain (MRLC) cDNA with EcoRI and BamHI restriction sites was cloned into a pHAT2 vector containing a histidine tag followed by an enhanced GFP (eGFP) sequence (obtained from Torsten Wittmann, UCSF). eGFP-MRLC was expressed in BL21(DE3) E. coli and purified on a Talon metal affinity resin (Clontech Laboratories, Inc.) according to the manufacturer's instructions. eGFP-RLC was co-microinjected with X-Rhodamine-conjugated actin at 1.0 and 0.5 mg/ml, respectively.

Microscopy

Time-lapse image sequences were acquired by spinning disk confocal microscopy utilizing a 100X/1.4 NA Plan Apo phase objective lens from Nikon. Images were acquired at 10 second intervals, with illumination at the 568 nm (X-Rhodamine) and 488 nm (eGFP) provided by a 2.5W KrAr laser (Coherent). Images were captured using a CoolSNAP-HQ2 camera from Photometrics.

Image Analysis

FSM time-lapse sequences were analyzed by custom-written software to obtain velocities of F-actin flow18, assembly/disassembly rate of F-actin network30 and velocities of cell edge movement9.

Force Reconstruction

The prediction of intracellular forces from F-actin network flows relied on a continuum-mechanical model that related forces inside the cell and at the cell boundary to network flows (Supplementary Note 4). Based on these equations, the problem was inverted, i.e. forces were derived from the measured flow fields (Supplementary Note 5). The solution of the inverse problem was determined by identifying the force field among many candidate fields that would produce a flow field most similar to the measured flow field. This approach optimized the spatial filtering of measurement noise, which would otherwise yield

nonsensical force spikes. The predicted intracellular forces were further decomposed into adhesion-dominant and contraction-dominant forces, using the *cone rule* (Fig. 2c) to distinguish the specific local relationships between force direction and network flow associated with adhesion and contraction forces (Supplementary Note 6).

Supplementary Material

Refer to Web version on PubMed Central for supplementary material.

Acknowledgment

We gratefully acknowledge funding from NIH R01 GM71868 and the Cell Migration Consortium, Grant No U54 GM064346 from NIGMS.

References

1. Pollard TD, Borisy GB. Cellular Motility Driven by Assembly and Disassembly of Actin Filaments. Cell. 2003; 112:453–465. [PubMed: 12600310]
2. Mogilner A, Oster G. Force Generation by Actin Polymerization II: The Elastic Ratchet and Tethered Filaments. Biophys. J. 2003; 84:1591–1605. [PubMed: 12609863]
3. Dickinson RB, Caro L, Purich DL. Force Generation by Cytoskeletal Filament End-Tracking Proteins. Biophys. J. 2004; 87:2838–2854. [PubMed: 15454475]
4. Hu K, Ji L, Applegate K, Danuser G, Waterman-Storer CM. Differential Transmission of Actin Motion within Focal Adhesions. Science. 2007; 315:111–115. [PubMed: 17204653]
5. Balaban NQ, et al. Force and focal adhesion assembly: a close relationship studied using elastic micropatterned substrates. Nature Cell Biology. 2001; 3:466–472. [PubMed: 11331874]
6. Beningo KA, Dembo M, Kaverina I, Small JV, Wang YL. Nascent focal adhesions are responsible for the generation of strong propulsive forces in migrating fibroblasts. J. Cell Biol. 2001; 153:881–887. [PubMed: 11352946]
7. Verkhovsky, AB.; Svitkina, TM.; Borisy, GG. Cell Behaviour: Control and Mechanism of Motility 207-222. Portland Press; London: 1999. Network contraction model for cell translocation and retrograde flow.
8. Gupton SL, Waterman-Storer CM. Spatiotemporal feedback between actomyosin and focal-adhesion systems optimizes rapid cell migration. Cell. 2006; 125:1361–1374. [PubMed: 16814721]
9. Machacek M, Danuser G. Morphodynamic Profiling of Protrusion Phenotypes. Biophys. J. 2006; 90:1439–1452. [PubMed: 16326902]
10. Dembo M, Wang YL. Stresses at the cell-to-substrate interface during locomotion of fibroblasts. Biophys J. 1999; 76:2307–2316. [PubMed: 10096925]
11. Munevar S, Wang Y.-l. Dembo M. Traction Force Microscopy of Migrating Normal and H-ras Transformed 3T3 Fibroblasts. Biophys. J. 2001; 80:1744–1757. [PubMed: 11259288]
12. Dembo M, Oliver T, Ishihara A, Jacobson K. Imaging the traction stresses exerted by locomoting cells with the elastic substratum method. Biophys. J. 1996; 70:2008–2022. [PubMed: 8785360]
13. Sterba RE, Sheetz MP. Basic laser tweezers. Methods in Cell Biology, Vol 55. 1998; 55:29–41.
14. Jiang G, Giannone G, Critchley DR, Fukumoto E, Sheetz MP. Two-piconewton slip bond between fibronectin and the cytoskeleton depends on talin. Nature. 2003; 424:334–337. [PubMed: 12867986]
15. Parekh SH, Chaudhuri O, Theriot JA, Fletcher DA. Loading history determines the velocity of actin-network growth. Nature Cell Biology. 2005; 7:1119–1123.
16. Prass M, Jacobson K, Mogilner A, Radmacher M. Direct measurement of the lamellipodial protrusive force in a migrating cell. J. Cell Biol. 2006; 174:767–772. [PubMed: 16966418]
17. Danuser G, Waterman-Storer CM. Quantitative Fluorescent Speckle Microscopy of Cytoskeleton Dynamics. Ann. Rev. of Biophys. Biomol. Struct. 2006; 35:361–387. [PubMed: 16689641]

18. Ji L, Danuser G. Tracking quasi-stationary flow of weak fluorescent signals by adaptive multi-frame correlation. J. Microscopy. 2005; 220:150–167.
19. Gardel ML, et al. Elastic Behavior of Cross-Linked and Bundled Actin Networks. Science. 2004; 304:1301–1305. [PubMed: 15166374]
20. Ponti A, Machacek M, Gupton SL, Waterman-Storer CM, Danuser G. Two distinct actin networks drive the protrusion of migrating cells. Science. 2004; 305:1782–1786. [PubMed: 15375270]
21. Delorme V, et al. Cofilin activity downstream of Pak1 regulates cell protrusion efficiency by organizing lamellipodium and lamella actin networks. Dev. Cell. 2007; 13:646–662. [PubMed: 17981134]
22. McGrath JL, Tardy Y, Dewey CF Jr. Meister JJ, Hartwig JH. Simultaneous measurements of actin filament turnover, filament fraction, and monomer diffusion in endothelial cells. Biophys J. 1998; 75:2070–2078. [PubMed: 9746549]
23. Ponti A, et al. Periodic patterns of actin turnover in lamellipodia and lamellae of migrating epithelial cells analyzed by Quantitative Fluorescent Speckle Microscopy. Biophys. J. 2005; 89:3456–3469. [PubMed: 16100274]
24. Galbraith CG, Yamada KM, Sheetz MP. The relationship between force and focal complex development. J. Cell Biol. 2002; 159:695–705. [PubMed: 12446745]
25. Tseng Y, et al. How actin crosslinking and bundling proteins cooperate to generate an enhanced cell mechanical response. Biochemical and Biophysical Research Communications. 2005; 334:183–192. [PubMed: 15992772]
26. Mahaffy RE, Park S, Gerde E, Kas J, Shih CK. Quantitative Analysis of the Viscoelastic Properties of Thin Regions of Fibroblasts Using Atomic Force Microscopy. Biophys. J. 2004; 86:1777–1793. [PubMed: 14990504]
27. Tseng Y, Kole TP, Wirtz D. Micromechanical mapping of live cells by multiple-particle-tracking microrheology. Biophys J. 2002; 83:3162–3176. [PubMed: 12496086]
28. Van Citters KM, Hoffman BD, Massiera G, Crocker JC. The role of F-actin and myosin in epithelial cell rheology. Biophysical Journal. 2006; 91:3946–3956. [PubMed: 16950850]
29. Bakolitsa C, et al. Structural basis for vinculin activation at sites of cell adhesion. Nature. 2004; 430:583–586. [PubMed: 15195105]
30. Ponti A, Vallotton P, Salmon WC, Waterman-Storer CM, Danuser G. Computational Analysis of F-Actin Turnover in Cortical Actin Meshworks Using Fluorescent Speckle Microscopy. Biophys. J. 2003; 84:3336–3352. [PubMed: 12719263]
31. Weisswange I, Bretschneider T, Anderson KI. The leading edge is a lipid diffusion barrier. J Cell Sci. 2005; 118:4375–4380. [PubMed: 16144867]
32. Prigozhina NL, Waterman-Storer CM. Decreased polarity and increased random motility in PtK1 epithelial cells correlate with inhibition of endosomal recycling. J Cell Sci. 2006; 119:3571–3582. [PubMed: 16931597]
33. Bretscher MS, Aguado-Velasco C. Membrane traffic during cell locomotion. Current Opinion in Cell Biology. 1998; 10:537–541. [PubMed: 9719876]
34. Hill TL, Kirschner MW. Bioenergetics and Kinetics of Microtubule and Actin Filament Assembly-Disassembly. International Review of Cytology-a Survey of Cell Biology. 1982; 78:1–125.
35. Gov NS, Gopinathan A. Dynamics of Membranes Driven by Actin Polymerization. Biophys. J. 2006; 90:454–469. [PubMed: 16239328]
36. Habermann B. The BAR-domain family of proteins: a case of bending and binding? EMBO Rep. 2004; 5:250–255. [PubMed: 14993925]
37. Waterman-Storer, CM. Fluorescent speckle microscopy (FSM) of microtubules and actin in living cells. In: Bonifacino, JS.; Dasso, M.; Harford, JB.; Lippincott-Schwartz, J.; Yamada, KM., editors. Current Protocols in Cell Biology. Wiley; New York: 2002.

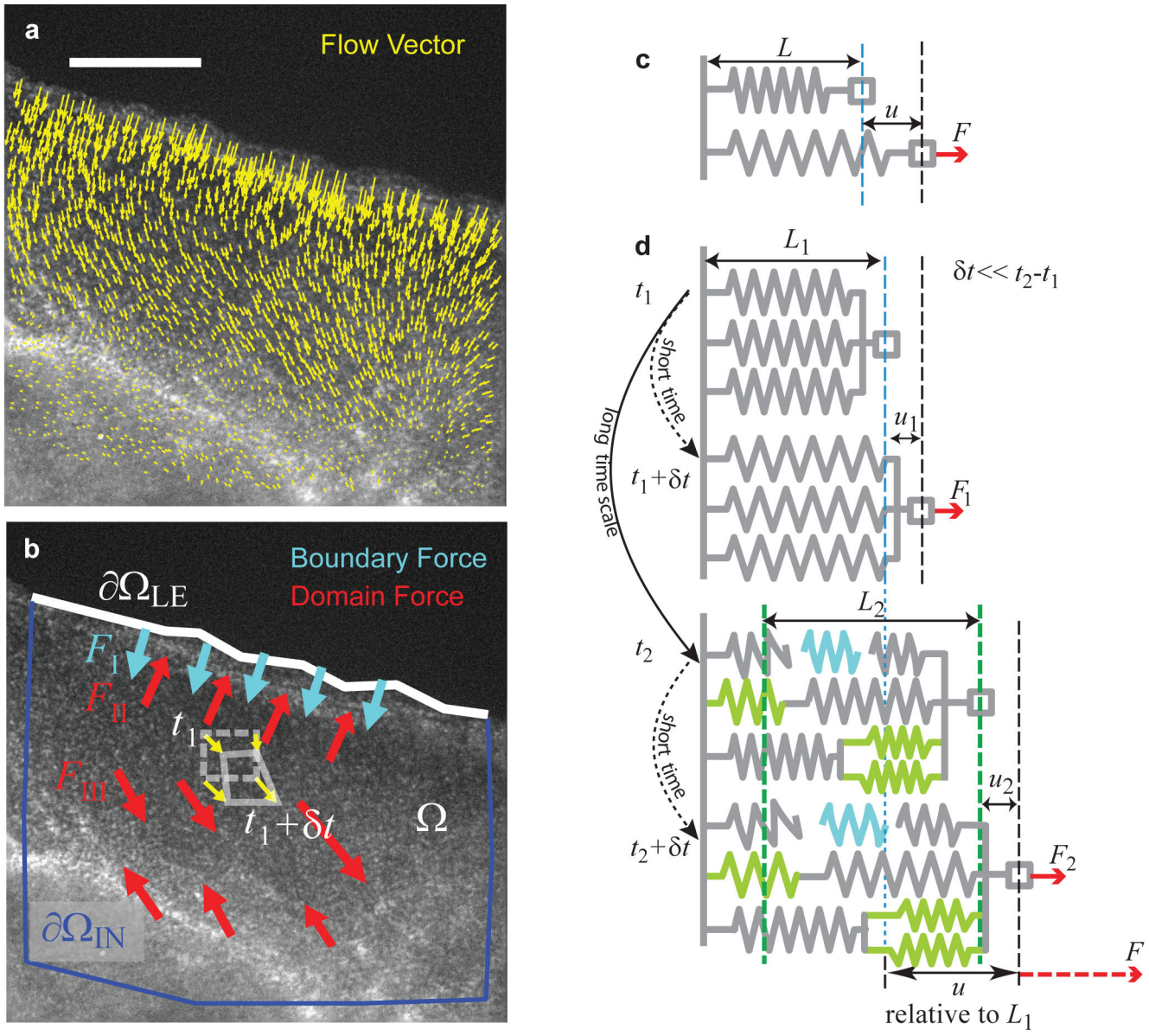

Figure 1.

Reconstruction of intracellular *force transients* from F-actin network flow. **(a)** Flow vectors measured by quantitative Fluorescent Speckle Microscopy (qFSM; Scale bar: 10 μm.). **(b)** Network flow is driven by forces at the cell boundary ($\partial\Omega_{LE}$) and by domain forces within lamellipodium and lamella (Ω). These forces generate transient deformations of the network, observed as spatial gradients in the displacement of fluorescent speckles over the time interval δt between two consecutive frames (illustrated by the transformation of a rectangle, dashed, into a polygon, solid gray lines. Network flows without spatial gradients indicate force free areas. **(c)** Force prediction from transient deformations of elastic spring. **(d)** Model of the F-actin network as a *transiently elastic* material. Over time scales $1s \leq \delta t \leq 10$ s, cross-linked F-actin networks deform predominantly elastically19. Thus, the material behaves like an ensemble of springs. At longer time scales t_2-t_1' δt, structures (cyan) break

while others (light green) form (plastic behavior). As a result pre-stress in the network is relaxed, which preserves the elastic constant and resting length of the spring ensemble ($L_1 \gg L_2$); yet, the relationship between the deformation u and the actual force change from t_1 to t_2 is lost. When the extension is fast compared to the time scale of remodeling, as from t_1 to $t_1+\delta t$ or from t_2 to $t_2+\delta t$ force changes can be inferred as $F_1=k\times u_1/L_1$ and $F_2=k\times u_2/L_2$.

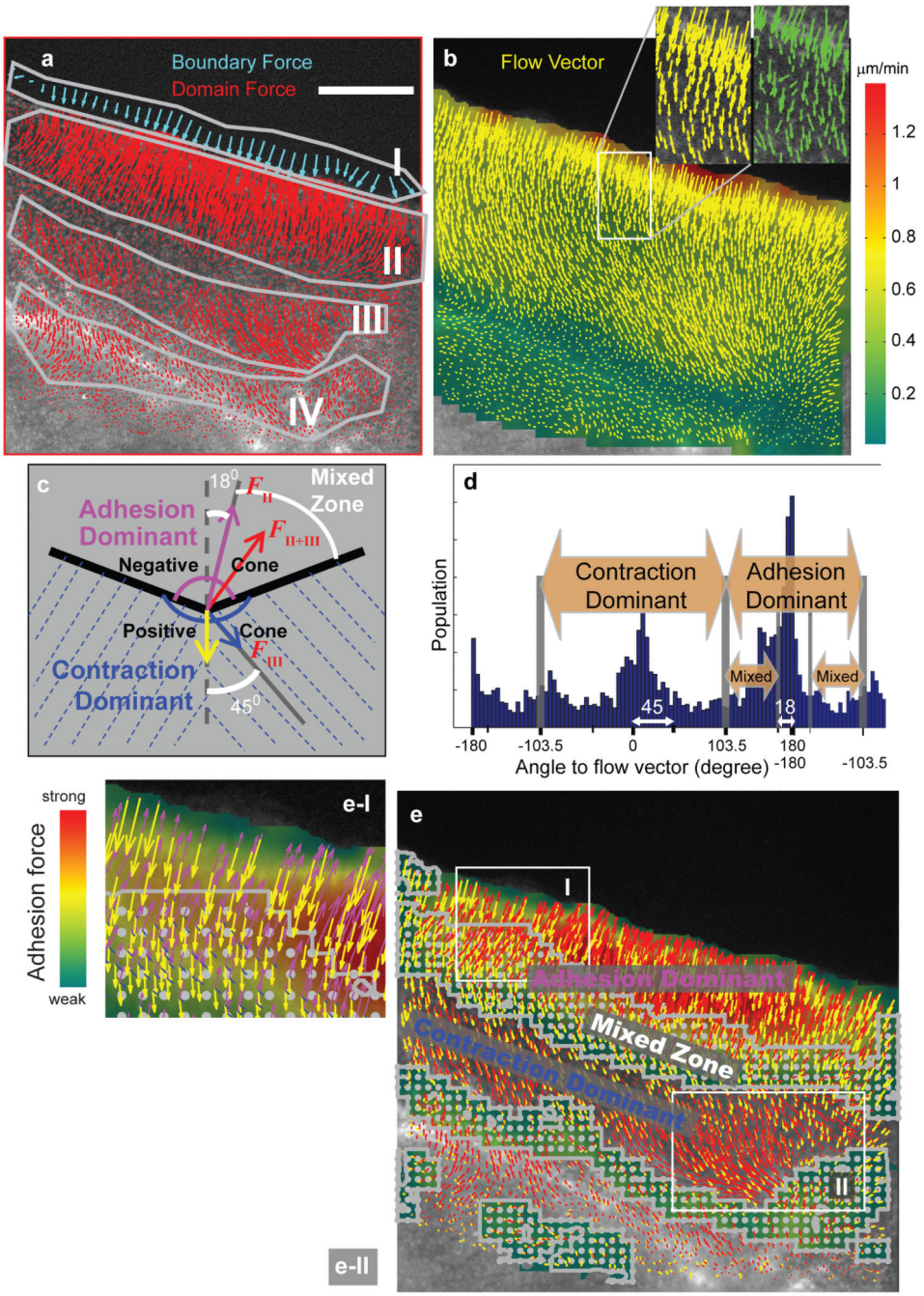

Figure 2.

Prediction of intracellular forces from F-actin network flow in Fig. 1. **(a)** Predicted force vectors (cyan: boundary forces; red: domain forces). Polygons I - IV highlight regions with different force characteristics (see text). **(b)** Flow field (yellow vectors) that would be produced by the predicted forces. Vectors are overlaid onto the color-coded speed map of the measured network flow. Insert: Comparison of the calculated (yellow) and measured (green) flow indicating the noise filtering during force reconstruction. **(c)** Cone rule to separate the contributions from adhesion and contraction to the predicted domain force. **(d)**

Distribution of angles between predicted force vectors and measured flow vectors. **(e)** Classification of predicted forces following the cone rule. In adhesion-dominant regions the magnitude of the adhesion force component is color-coded. Positions with significant contributions from both adhesion and contraction (mixed zone) are indicated by grey dots. Insets e-I and e-II show regions of mixed adhesion and contraction forces, respectively. Mixed forces are further decomposed into a contraction component (blue) and adhesion component (magenta). Scale bar in a: 10 μm.

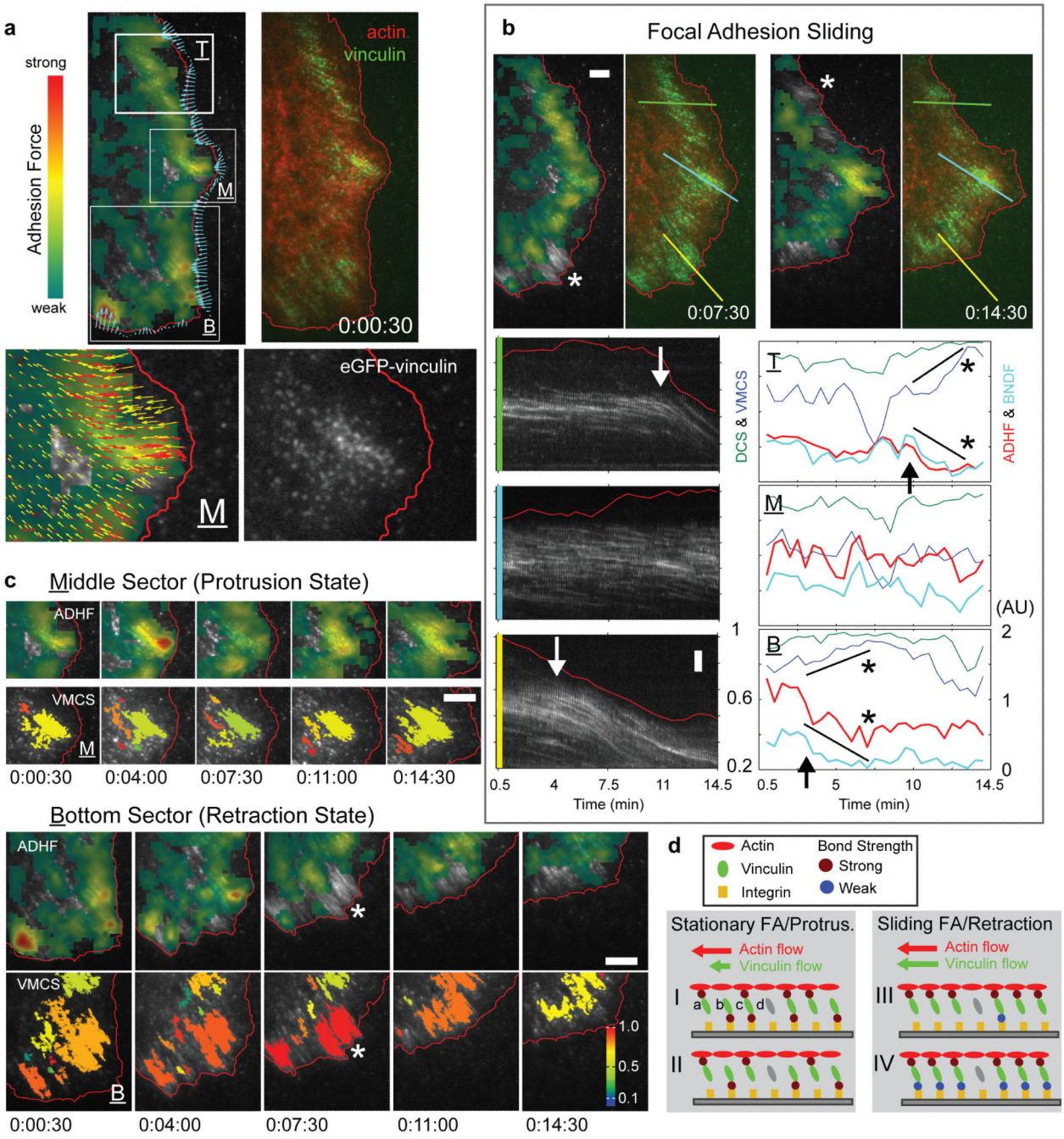

Figure 3.

Relationship between predicted adhesion forces and F-actin-vinculin interactions during protrusion and retraction. **(a)** *Top-left panel*: adhesion force magnitude (color-coded) and boundary force (cyan vectors); *Top-right panel*: dual-color FSM image of F-actin (red) and vinculin (green) (see Video 2). *Bottom-left panel*: Zoom of the middle sector M showing F-actin flow (yellow vectors), adhesion forces (red vectors) overlaid to adhesion force magnitude (color-coded). *Bottom-right panel:* eGFP-vinculin signal. **(b)** *Top row:* Adhesion force magnitude (color-coded) and F-actin/vinculin signal in two time-points between which

the cell edge in the bottom sector (first) and top sector (second) retracts and the adhesions slide (asterisk). *Bottom-left column*: Kymograph display of vinculin signal along three profiles indicated in the top panels. *Bottom-right column*: Time courses of the average adhesion (ADHF; red) and boundary forces (BNDF; cyan) in the Top, Bottom and Middle sectors. Also shown are time courses of the direction-coupling score (DCS, green) and the velocity-magnitude-coupling score (VMCS, blue) of F-actin and vinculin speckle motion4. Arrows: onset of decreasing adhesion and boundary forces, which correlates in time with increased motion coupling of F-actin and vinculin speckles. Asterisks: time-points of minimal adhesion forces (correspond to asterisks in top row). **(c)** Time montages of the adhesion force (ADHF) and the velocity magnitude coupling score (VMCS) in the middle and bottom sectors. **(d)** Models of a vinculin-mediated clutch. Scale bars: 5 μm.

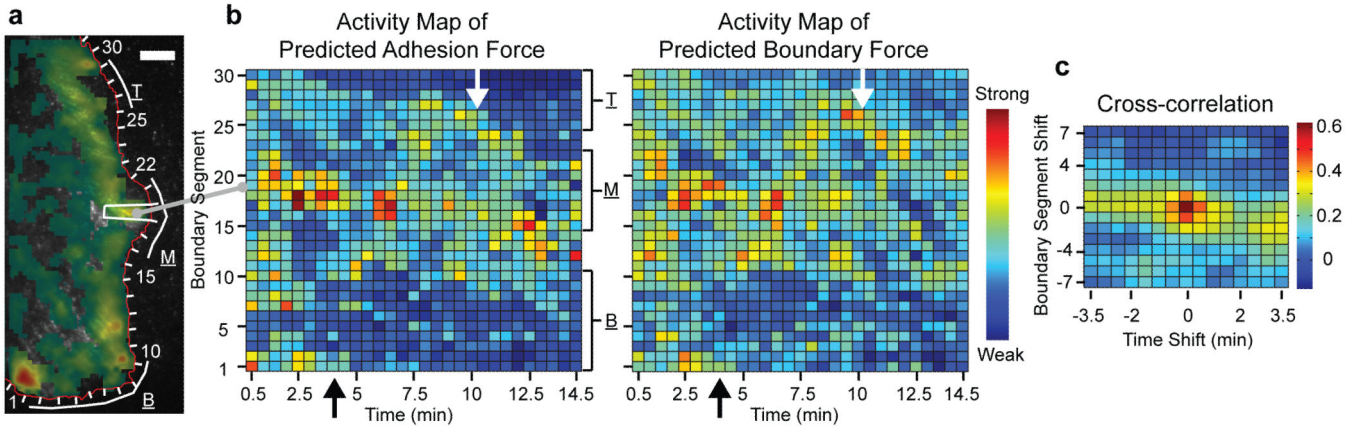

Figure 4.

Predicted adhesion force transients near the leading edge are synchronized in time and co-localized in space with predicted boundary force transients. **(a)** Definition of edge-tracking probing windows (see Video 3). Per window and time-point averaged boundary and adhesion force transients are calculated. **(b)** Construction of activity maps of predicted adhesion (left) and boundary forces (right). For one time-point, predicted force magnitudes are collected in all probing windows along the cell edge and copied into one column of the activity map (see example of probing window #19 mapped into the first column). The procedure is repeated for the entire time-lapse sequence to reveal the spatiotemporal organization of force development. Arrows: concurrent dropping of adhesion and boundary forces at the time-points adhesion begin to slide (cf. Fig. 3b). **(c)** Cross-correlation of adhesion and boundary force activity maps. Scale bar in a: 10 μm.

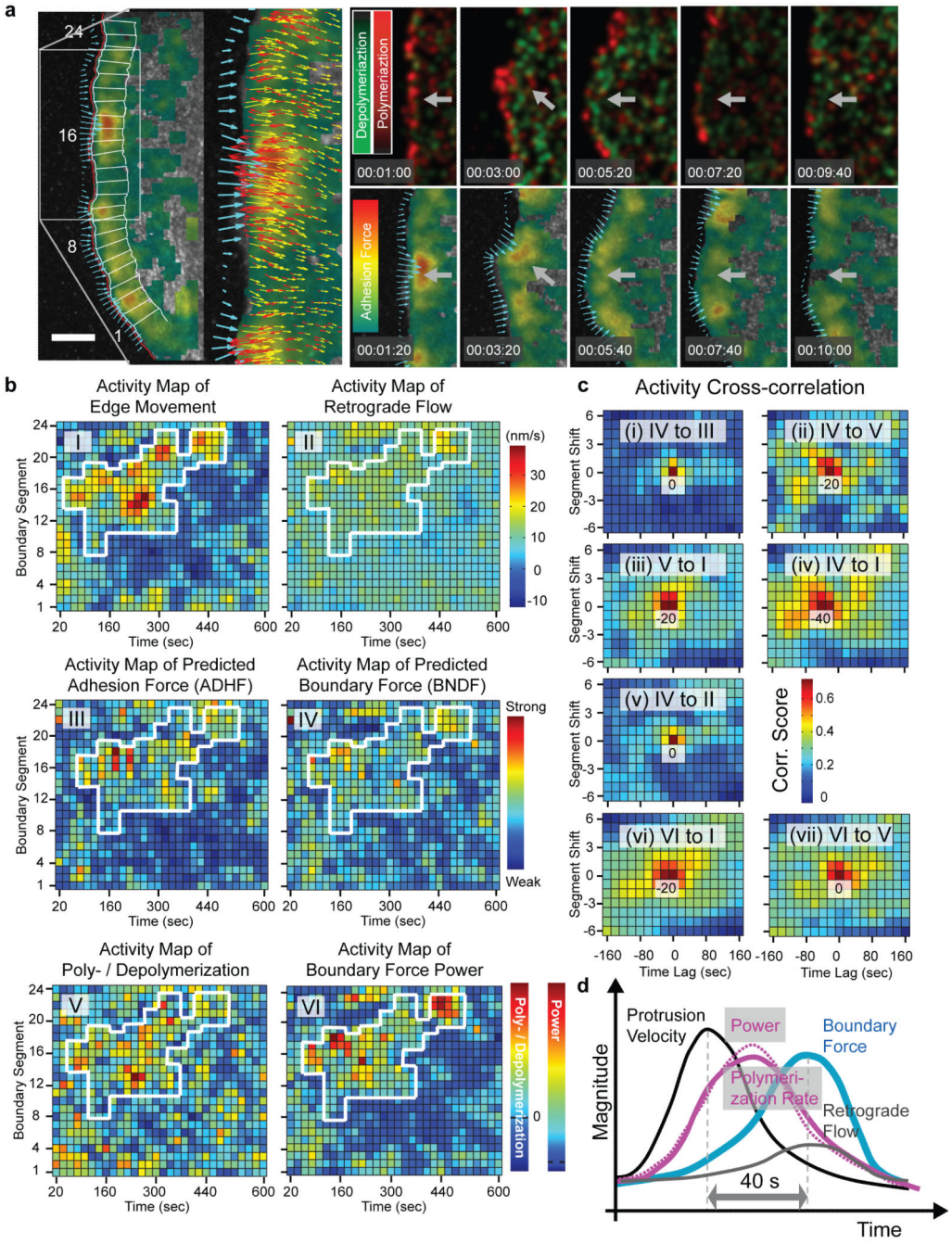

Figure 5.

Coordination of predicted force transients during cell protrusion with F-actin assembly and edge movement. **(a)** *Left panel*: Boundary forces (cyan vectors) and adhesion force magnitudes (color-coded) at the leading edge of a protruding epithelial cell. 24 probing windows (overlaid boxes) were used to construct the activity maps shown in b. *Zoom in*: Predicted boundary (cyan) and adhesion (red) force vectors, and F-actin flow vectors (yellow) overlaid to the adhesion force magnitude (color-coded) in protruding sector of the cell edge. *Right panel*: Time montage of rates of F-actin polymerization (red) and

depolymerization (green, top row); and of adhesion force magnitude (color-coded) and boundary forces (cyan vectors, bottom row) during a protrusion event. The two time series are shifted by 20 sec to account the delay in predicted adhesion/boundary force transients relative to rate changes in F-actin turnover (see text; see Video 4 for time-resolved force and assembly maps). **(b)** Activity maps of (I) cell edge movement, (II) velocity of F-actin retrograde flow, (III) predicted adhesion force, (IV) predicted boundary force, (V) rate of F-actin polymerization and depolymerization, and (VI) power (boundary force times the sum of the speeds of cell edge protrusion and retrograde flow). **(c)** Cross-correlation between activities. Negative time lags indicate that the first activity is delayed relative to the second activity. **(d)** Event sequence during a protrusion cycle. Scale bar in a: 5 μm.